RSC Advances

PAPER

Cite this: *RSC Adv.*, 2023, **13**, 10818

Sputtered Cu-doped NiO thin films as an efficient electrocatalyst for methanol oxidation†

Mohamed Sh. Abdel-wahab, * Hadeer K. El Emam and Waleed M. A. El Rouby

The efficient electrocatalysts for direct methanol oxidation play an essential role in the electrochemical energy conversion systems for their application in a wide range of portable applications. Consequently, Cu-doped NiO thin films on fluorine-doped tin oxide (FTO) were successfully prepared by the co-sputtering deposition technique, using various deposition times (300, 600, 900, and 1200 seconds), and producing films of different thicknesses (30, 55, 90, and 120 nm, respectively). X-ray diffraction (XRD) revealed the ideal crystallinity of the structure of the prepared films and was used to observe the effect of the thickness of the films on the crystal size. Energy-dispersive X-ray spectroscopy (EDS) confirmed the purity of the deposited film without any contamination. Field emission scanning electron microscopy (FESEM) images confirmed the film thickness increase with increasing deposition time. The surface roughness value of the Cu–NiO 1200 film was found to be 3.2 nm based on the atomic force microscopy (AFM) measurements. The deposited thin films of different thicknesses have been used as electrocatalysts for methanol oxidation at various concentrations of methanol (0, 0.5, 1, and 2 M), and displayed the highest electrocatalytic performance in 1 M methanol. Cu-doped NiO thin films have the advantage as electrocatalysts where they can be used directly without adding any binder or conducting agents, this is because Cu-doped NiO is deposited with high adhesion and strong electrical contact to the FTO substrate. A clear impact on the catalytic activity with increasing film thickness and a correlation between the film thickness and its catalytic activity was observed. The current density increased by about 60% for the Cu–NiO 1200 sample compared to Cu–NiO 300 sample, with the lowest onset potential of 0.4 V *vs.* Ag/AgCl. All deposited thin films of different thicknesses exhibited high stability at 0.6 V in 1 M methanol. This will open the window toward using physical deposition techniques for optimizing the electrocatalytic activity of different catalysts for electrocatalytic applications.

Received 18th January 2023
Accepted 27th March 2023

DOI: 10.1039/d3ra00380a

rsc.li/rsc-advances

1. Introduction

Direct methanol fuel cell development (DMFC) has gotten a lot of interest because it is considered an alternate power source to traditional energy-generation devices.[1] Moreover, DMFCs have many advantages, such as being environmentally friendly power sources for stationary electronic devices, having high energy density, working at low temperatures, and producing minimal pollutant emission.[2]

Methanol is oxidized directly at the anode by CO oxidation, as shown in the following reactions:[3]

$$CH_3OH \rightarrow CH_3OH_{ads} \quad (1)$$

$$CH_3OH_{ads} \rightarrow CO_{ads} + 4H^+ + 4e^- \quad (2)$$

$$CO_{ads} + H_2O \rightarrow CO_2 + 2H^+ + 2e^- \quad (3)$$

$$CH_3OH + H_2O \rightarrow CO_2 + 6H^+ + 6e^- \quad (4)$$

Methanol can be oxidized in both acidic and alkaline environments.[4] But in each case, the complete oxidation of CH_3OH to CO_2 is usually sluggish, and the reactions will only complete more quickly when higher potentials are applied.[5] So many efforts have been made to develop materials that can catalytically oxidize methanol at a lower overpotential,[6] consequently enhancing the efficiency and power of fuel cells. Several electrode materials based on platinum electrodes were extensively utilized as a catalyst for the electrochemical oxidation of methanol.[7–9] However, one of the limitations is that Pt is readily poisoned by adsorbed CO produced during methanol oxidation, which inhibits the Pt active sites. Furthermore, Pt is a rare earth element and costly. Hence, alternative metals that maintain a high catalytic activity level have been taking great interest.[10–13]

There are many ways to improve the electrocatalytic activity of DMFC; depending on synthetization, the anode is constructed of an alloy of transition metals and precious metals

Materials Science and Nanotechnology Department, Faculty of Postgraduate Studies for Advanced Sciences, Beni-Suef University, Beni-Suef 62511, Egypt. E-mail: mshaabancnt@psas.bsu.edu.eg

† Electronic supplementary information (ESI) available. See DOI: https://doi.org/10.1039/d3ra00380a

alloy. Among the transition metals that have been used for this target Co,[14] Ni,[15] Mn,[16] Ce,[17] Fe,[18] and Cu[19] are the most common. Nickel-based nanomaterials have attracted the interest of many researchers because they are less expensive and have shown high stability in alkaline mediums.[20] Moreover, Ni can prevent itself from oxidation by forming $Ni(OH)_2$ through the adsorbed OH^- ions; thus, it makes the surface static.[21] However, various limits restrict the use of transition metal-based anodes in DMFCs, such as having high onset potential in methanol oxidation reaction (MOR) and loss of catalyst systems.[22–25] Ni-based electrodes have high activity for methanol oxidation-reduction, so Ni^{2+} and Ni^{3+} species have been used for NiO electrodeposition on various types of substrate electrochemically.[25–27] Electrocatalysts based on Cu have a lower affinity for carbon monoxide (CO) than Ru, Rh, Pd, and Pt. Consequently, more materials related to Cu have been described as acceptable electrocatalysts for DMFC in alkaline environments.[28]

The catalytic activity may be increased *via* metal doping, where the insertion of a foreign atom into the lattice of the catalyst.[29] The substitution of dopants for parental atoms in host materials is a successful technique for tuning their physicochemical properties, such as modulating energy levels and the electronic structure, which increases the electrical conductivity of the catalyst, consequently improving the charge transfer mechanisms and corrosion resistance, leading to high stability. This method allows us to generate effective electrocatalysts inexpensively.[29–31]

Herein in this work, Cu-doped NiO films have been deposited on the FTO substrate at various deposited times (300, 600, 900, 1200 seconds) using a co-sputtering deposition method. Based on our knowledge, such co-sputtering deposited films have not been studied before as electrocatalysts for methanol oxidation. The effect of Cu-doped NiO film thickness on electrocatalytic activity was studied and evaluated. The results revealed that increasing the film thickness improves the catalytic activity and exhibit excellent stability for MOR. The charge transfer becomes faster because nickel has an optimal electrochemical activity for MOR. This will open the window toward using physical deposition techniques for optimizing the electrocatalytic activity of different catalysts for different applications.

2. Materials and methods

2.1. Preparation conditions of the deposited Cu-doped NiO thin films

The co-sputtering deposition process is one of the most promising techniques for tuning and controlling the percentage of dopant atoms in the hosting thin films. Using DC/RF sputtering system (Syskey Technologies, Taiwan), 5.83 wt% Cu-doped NiO thin films have been prepared on both glass slides and fluorine-doped tin oxide with different thicknesses 30, 55, 90, and 120 nm by varying the deposition time from 300, 600, and 900 to 1200 s, respectively. Before the deposition process, the glass slides and FTO substrates were subjected to different cleaning steps using acetone and ethanol and dried using nitrogen gas.

Table 1 Thin film preparation conditions

No	Deposition parameters	Value
1	Base pressure	9×10^{-6} Torr
2	Operating pressure	5×10^{-3} Torr
3	Deposition time	300, 600, 900, and 1200 s
4	Substrate temperature	25 °C
5	DC power for Ni target	200 W
6	RF power for Cu target	20 W
7	Oxygen flow rate	10 SCCM
8	Argon flow rate	20 SCCM
9	Substrate rotation	15 rpm
10	Target-substrate distance	14 cm

The preparation conditions for the prepared samples are summarized in Table 1.

2.2. Characterization of the prepared thin films

X-ray diffraction (Shimadzu LabX-XRD-6000, Japan) at 40 kV/40 mA with Cu–K radiation (0.154056 nm) is utilized to identify the crystalline phases of thin films. Atomic force microscopy (AFM, Omicron-UHV-VT-AFMXA) is used to detriment the roughness of the surface. Field emission scanning electron microscopy (FESEM, Zeiss sigma 500 VP, Germany) was used to investigate the morphology and the crystal structure. Energy dispersive X-ray fixed on the SEM was also used to analyze the elemental composition and map the elements on the film's surface. A UV-Vis-spectrophotometer (PerkinElmer Lambda 750; Massachusetts, USA) has been used to characterize the prepared films' optical properties.

2.3. Electrochemical measurements

All films were tested for electrocatalytic activity toward methanol oxidation in an alkaline medium in a three-electrode system at room temperature. The reference electrode and counter electrodes were Ag/AgCl and Pt wire, respectively, the prepared films was used as working electrodes, and 0.5 M KOH was used as the electrolyte solution. The electrocatalytic activity was tested in a pure 0.5 M KOH and in different methanol concentrations (0.5, 1, 2 M) by mixing the calculated volume with the KOH solution. All electrochemical measurements were carried out with the help of an Autolab (PGSTAT302N) potentiostat (Metrohm). The measurements were made using cyclic voltammetry (CV) at scan rates ranging from 10 to 100 mV s^{-1}, electrochemical impedance spectroscopy (EIS) at 0.6 and amplitude of 10 mV, and chronoamperometry (CA) as indicator for the samples stability, was recorded at 0.6 V for 1 h. The best sample of the highest electrocatalytic activity (Cu–NiO 1200) was tested over 6 h. Based on the geometric surface area of the used electrodes, the current densities have been normalized.

3. Results and discussion

3.1. Structural analysis

The XRD patterns presented in Fig. 1 illustrate the crystallinity of all prepared materials. The ICDD card [01-089-3080] matched

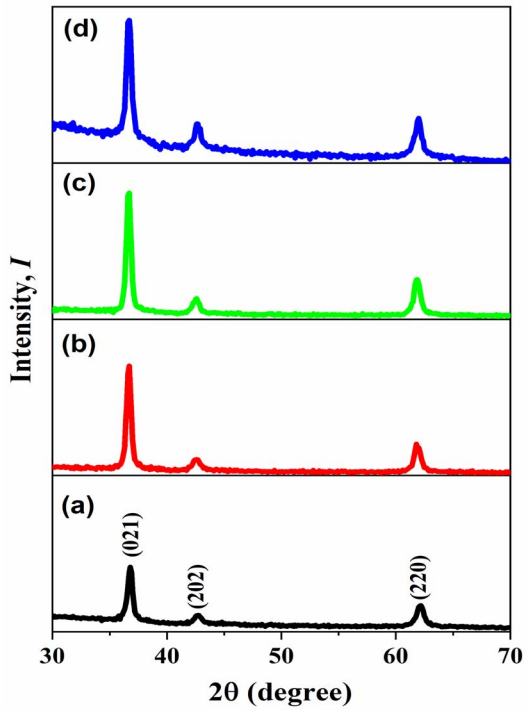

Fig. 1 X-ray diffraction of NiO–Cu thin films deposited by different time (a) 300, (b) 600, (c) 900, (d) 1200 Sec.

the diffraction peaks, identifying the space group $R\bar{3}m$ (166) of a single phase of nickel oxide with a trigonal structure. However, when nickel oxide was doped by copper, there are no other peaks appeared different from the pure nickel oxide peaks, which are located at (021), (202), and (220) because the ionic radius in Ni and Cu is the same approximately which is 0.072 nm.[32] On the other hand, the peaks intensity were increased when the thickness of films increased due to the amount of X-ray absorption increased. Debye Scherrer's equation calculated the average crystal size D.[33]

$$D = \frac{0.94\lambda}{\beta \cos \theta} \quad (5)$$

where D is crystal size, λ is the used wavelength of the X-ray, β is the diffraction peak width, and θ is the diffraction angle. Also, the following formula (6) and (7) were used to compute dislocation density δ and lattice strain ε.[34]

$$\delta = \frac{n}{D^2} \quad (6)$$

$$\varepsilon = \frac{\beta \cos \theta}{4} \quad (7)$$

The structural characteristics of the prepared films with various thicknesses, such as average crystallite size, dislocation density, and lattice strain, are shown in Table 2. The obtained result revealed the effect of the thickness on the crystal size, where NiO–Cu1200 has the biggest size equal to 16.73 nm, and NiO–Cu300 has 14.61 nm.

3.2. Morphological analysis

Fig. 2 shows FESEM images of all thin films (Cu-doped NiO) with various deposition times (300, 600, 900 and 1200 seconds). The images clarify that the films became rougher with increasing the deposition time; besides, more particle agglomerations are shown. The morphology consists of grain particles with non-homogeneous sizes. It is also clear that the prepared films are free of defects, and with increasing the deposition time, the particles became more condensed due to the deposition of more particles on each other. The elemental analysis of deposited films NiO–Cu 300, NiO–Cu 600, NiO–Cu 900, and NiO–Cu 1200 were analyzed by EDS as shown in Fig. 3(a–c), S1(a–c), S2(a–c), and S3(a–c).† It clarifies the purity of the deposited NiO–Cu thin films, which only contain spectra for Ni, O, and Cu elements. To identify the distribution of different elements and to indicate the successful doping, elemental mapping has been conducted for all samples, as seen in Fig. 3d,

Table 2 The structural characteristics of the prepared thin films

Material	2θ°	(hkl)	Crystallite size, (nm)	Dislocation density	Lattice strain
NiO–Cu 300	36.79	(021)	18.03	3.07×10^{-3}	1.92×10^{-3}
	42.69	(202)	12.18	6.74×10^{-3}	2.84×10^{-3}
	62.08	(220)	13.64	5.37×10^{-3}	2.54×10^{-3}
Mean value			**14.61**	$\mathbf{5.06 \times 10^{-3}}$	$\mathbf{2.43 \times 10^{-3}}$
NiO–Cu 600	36.66	(021)	18.87	2.80×10^{-3}	1.83×10^{-3}
	42.59	(202)	11.00	8.25×10^{-3}	3.15×10^{-3}
	61.80	(220)	15.19	4.33×10^{-3}	2.28×10^{-3}
Mean value			**15.02**	$\mathbf{5.12 \times 10^{-3}}$	$\mathbf{2.42 \times 10^{-3}}$
NiO–Cu 900	36.65	(021)	18.23	3.01×10^{-3}	1.90×10^{-3}
	42.60	(202)	12.60	6.29×10^{-3}	2.75×10^{-3}
	61.73	(220)	16.91	3.49×10^{-3}	2.05×10^{-3}
Mean value			**15.91**	$\mathbf{4.26 \times 10^{-3}}$	$\mathbf{2.23 \times 10^{-3}}$
NiO–Cu 1200	36.64	(021)	17.47	3.27×10^{-3}	1.98×10^{-3}
	42.56	(202)	15.72	4.05×10^{-3}	2.20×10^{-3}
	61.90	(220)	17.01	3.46×10^{-3}	2.04×10^{-3}
Mean value			**16.73**	$\mathbf{3.59 \times 10^{-3}}$	$\mathbf{2.07 \times 10^{-3}}$

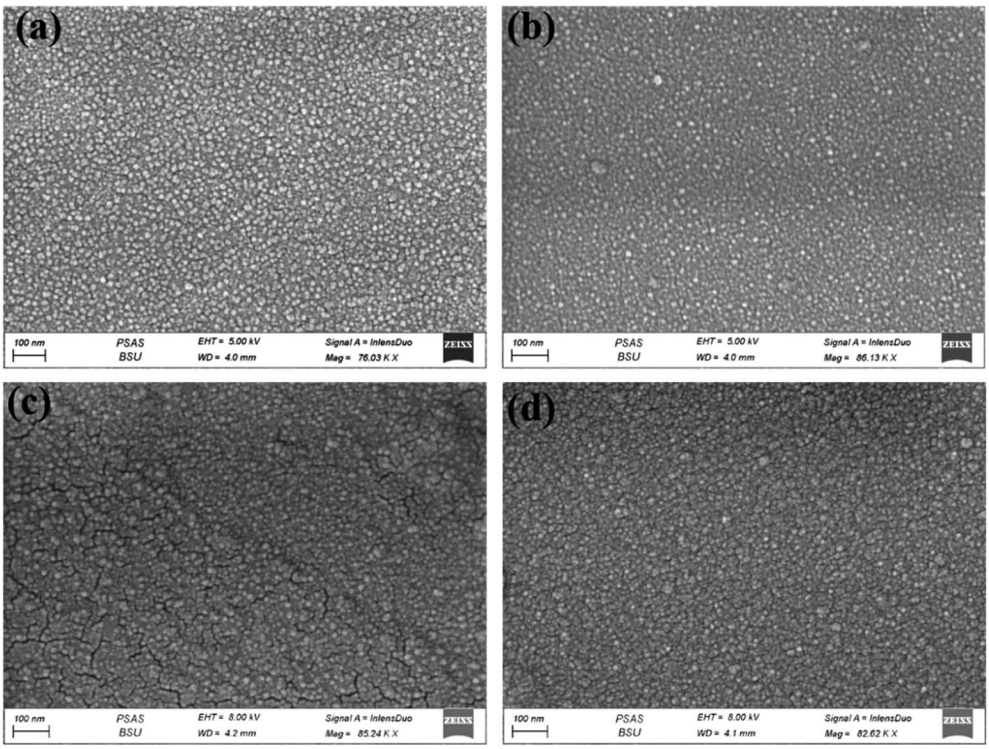

Fig. 2 FESEM images of NiO–Cu thin films deposited for (a) 300, (b) 600, (c) 900, (d) 1200 s.

S1d, S2d, and S3d.† It is seen that there is a homogeneous distribution of the elements all over the surface of the deposited films.

To specify the effect of deposition time on the obtained film thickness, SEM images have been taken under a setting of 45 degrees, as seen in Fig. 4. It's clear that the thickness of the thin

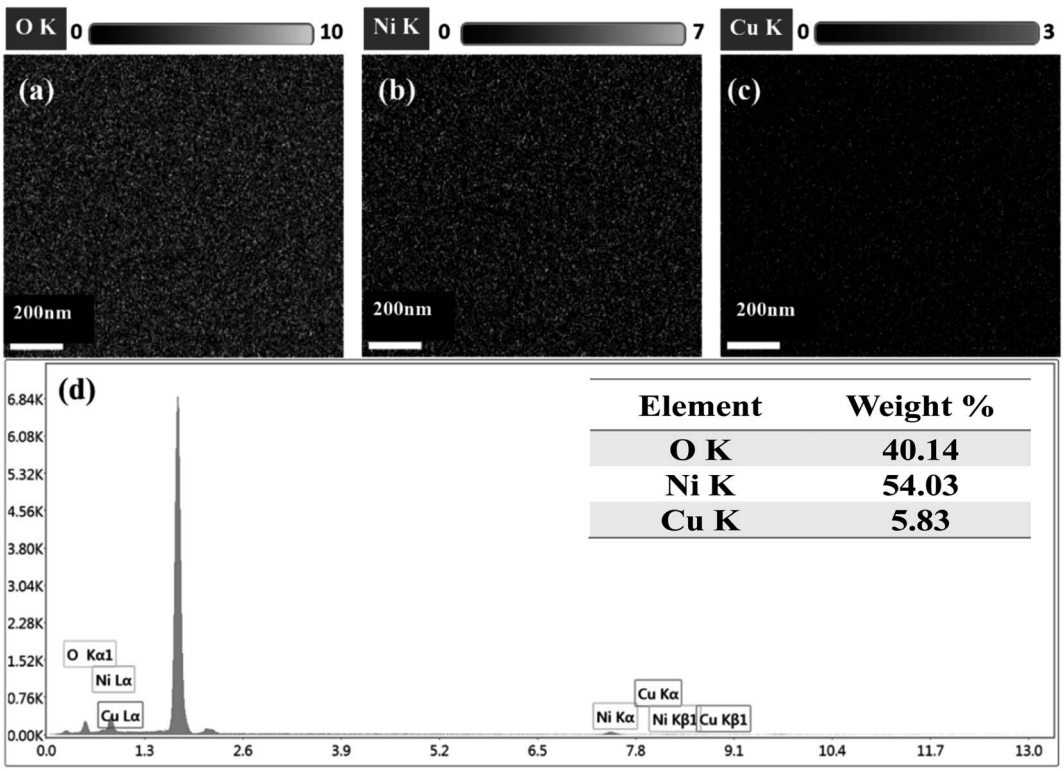

Fig. 3 EDS spectrum of NiO–Cu 300, (a) O, (b) Ni, (C) Cu, and (d) elemental mapping images of Ni, O, and Cu and.

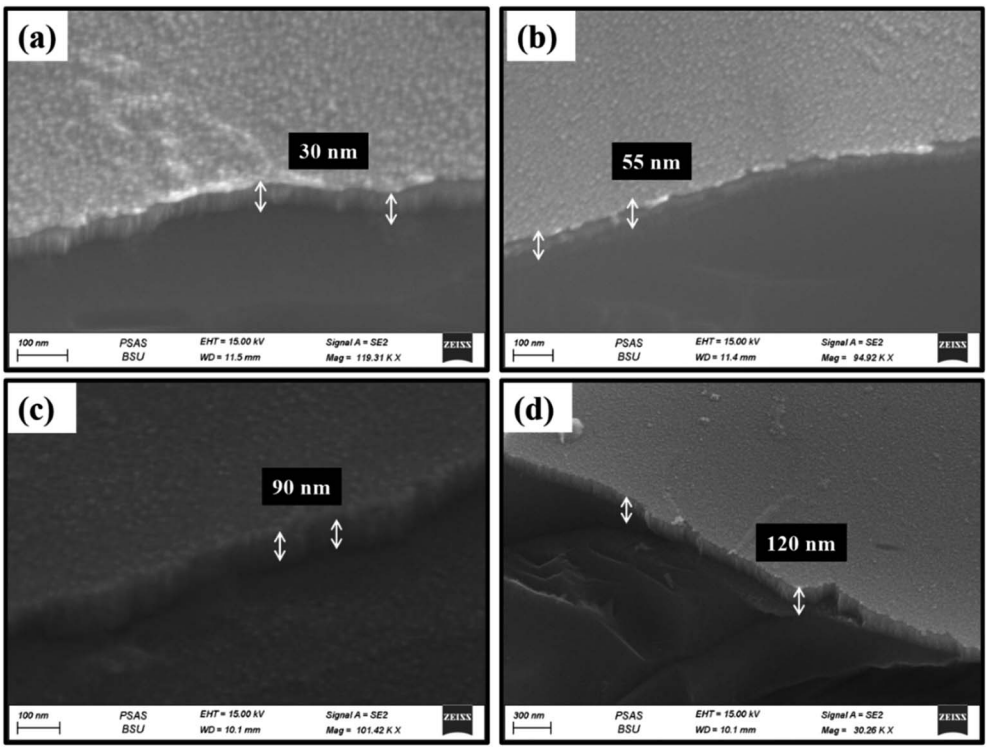

Fig. 4 Thickness of the thin films is presented by FESEM (a) NiO–Cu 300, (b) NiO–Cu 600, (c) NiO–Cu 900, (d) NiO–Cu 1200.

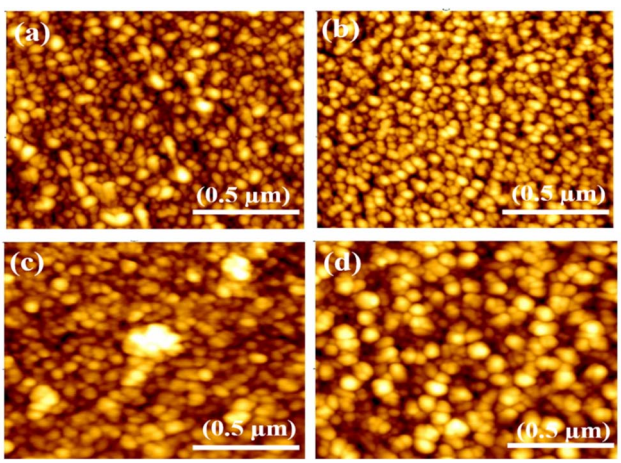

Fig. 5 AFM images (a) NiO–Cu 300, (b) NiO–Cu 600, (c) NiO–Cu 900, (d) NiO–Cu 1200.

Table 3 The prepared thin films' grain size and surface roughness

The prepared films	Grain size (nm)	Surface roughness (nm)
NiO–Cu 300	52	1.9
NiO–Cu 600	57	2.2
NiO–Cu 900	69	2.6
NiO–Cu 1200	75	3.2

films increases by increasing the deposition time during the preparation. For NiO–Cu 300, the thickness is about 42 nm (Fig. 4a), while for NiO–Cu 1200 sample, the thickness is about 120 nm (Fig. 4d), which increased by three times.

Atomic force microscopy is utilized to measure the grain size and illustrate the surface roughness of synthesized films, as in Fig. 5. The size of the grains was observed that increase with increasing the thickness (deposition time) of the films, which was recorded (52, 57, 69 and 75 nm) for NiO–Cu 300, NiO–Cu 600, NiO–Cu 900, and NiO–Cu 1200 respectively. The AFM shows that nanocrystalline sizes in Table 3 are larger than the typical crystal size derived from the XRD peak width in Table 2 due to many nanocrystallized having the same plane and orientation were merged to create nanocrystals. According to Gibbs free energy, the nanoparticles of small-sized surfaces are relatively high due to the ratio of the huge surface to the volume; therefore, the small particles agglomerate to reduce the Gibbs free energy and achieve stability for the surface.[35] In addition, thin films' surface roughness increases with the increasing deposition time, as seen in Table 3.

3.3. Optical analysis

Fig. 6(a) illustrates the evaluations of the optical absorption using UV-vis spectroscopy. There is a noticeable and predicted decline in transmittance with increasing film thickness, which might be due to easier charge transfer. Moreover, the Tauc relation, as shown in eqn (8) was utilized to calculate the bandgap of films.[36]

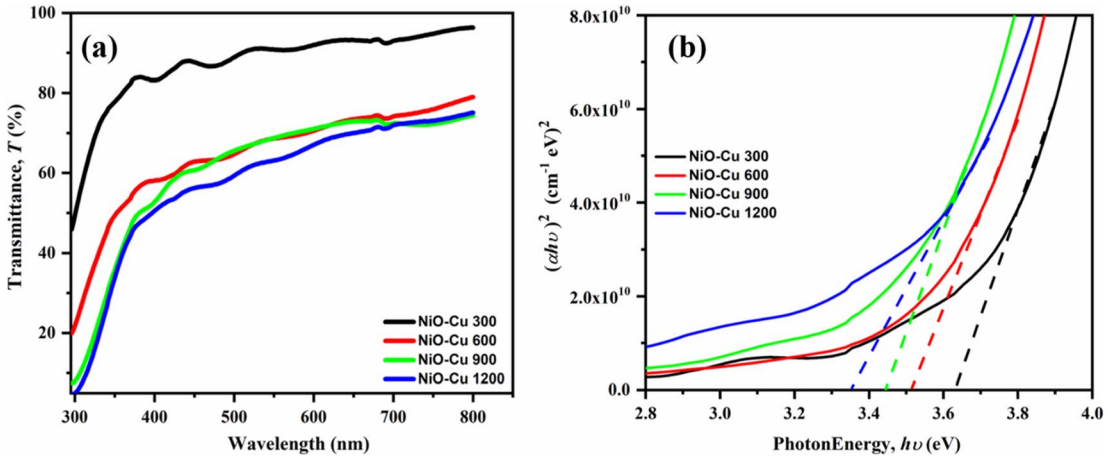

Fig. 6 (a) Optical transmittance, and (b) optical band gaps of the prepared thin films.

$$\alpha = \frac{A}{h\nu}(h\nu - E_g)^n \quad (8)$$

where A is a constant, $h\nu$ is the incident photon's energy, and the absorbance coefficient is (α) and (n) is perhaps equal to 1/2 or 2 for the direct and indirect band gap, respectively, according to the selection rules of quantum for various materials.

The junction point between the linear regions and the photon energy $(h\nu)$ axis was the value of the films' band gap. It is

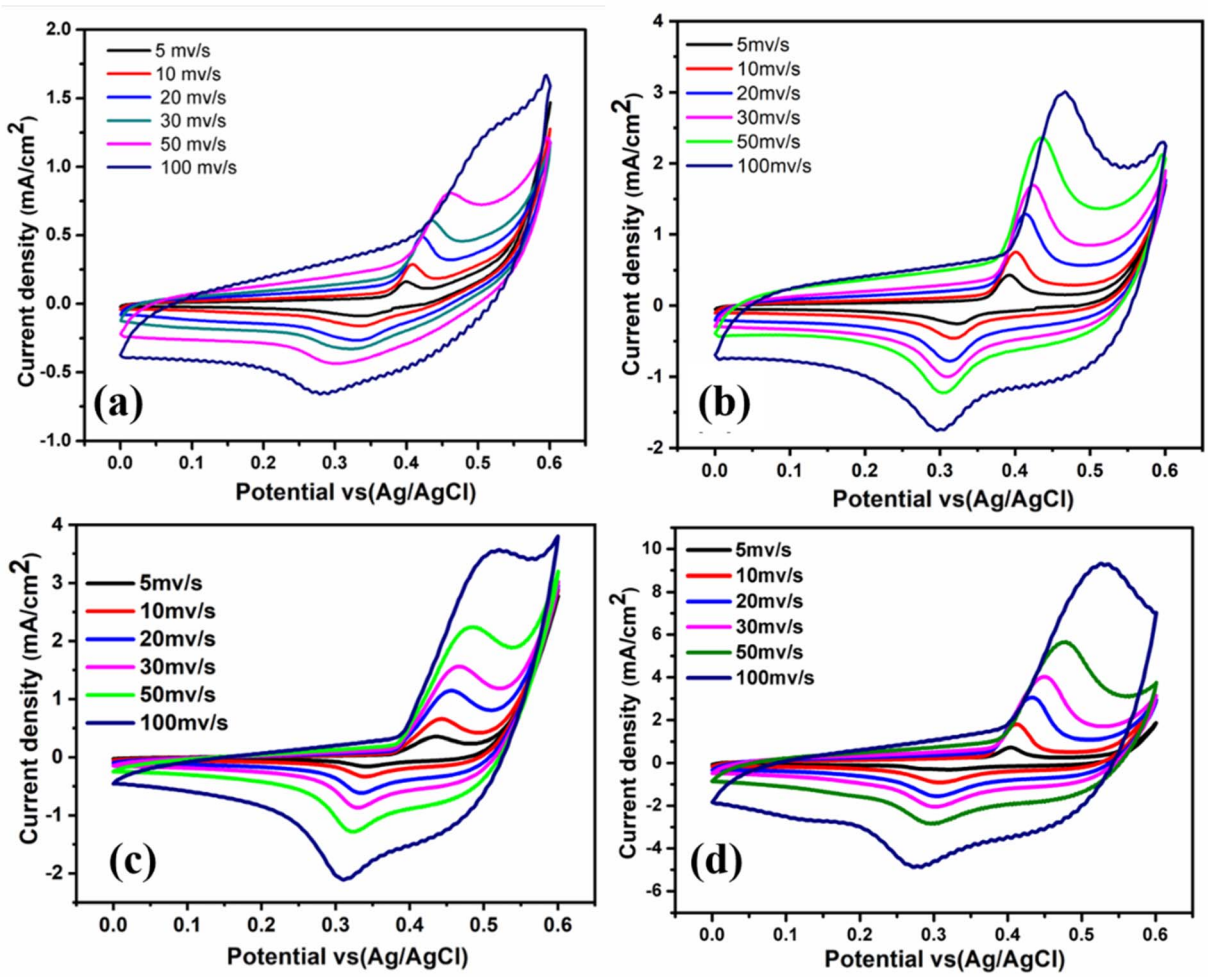

Fig. 7 Cyclic voltammograms for all films in 0.5 M KOH at room temperature with different scan rates (a) NiO–Cu 300, (b) NiO–Cu 600, (c) NiO–Cu 900, (d) NiO–Cu 1200.

Table 4 The current density of all samples at different scan rates in 0.5 M KOH

Scan rate (mV s^{-1})	Current density (mA cm^{-2})			
	NiO–Cu 300	NiO–Cu 600	NiO–Cu 900	NiO–Cu 1200
5	0.98	1	2.72	1.88
10	1.12	1.1	2.85	2.5
20	1.2	1.3	3	2.9
30	1.28	1.7	3.3	4.1
50	1.4	2.4	3.5	5.8
100	1.67	3	3.8	9.5

noted that as the thickness of the thin films increases, the band gap values decrease (Fig. 6(b)). According to the recorded values for NiO–Cu 1200, NiO–Cu 900, NiO–Cu 600, and NiO–Cu 300, the band gaps were (3.35, 3.44, 3.51, 3.63 eV), respectively. The reason may be linked to improvements in crystallinity and morphological alterations, as mentioned above in the XRD and FESEM; furthermore, some literature[36–38] endorses that the localized states in the band structure may merge with the band edges when the film's thickness grows, reducing the band gap.

3.4. Electrocatalytic activity

Fig. 7 illustrates the CV curves of all films in 0.5 M KOH electrolyte at different scan rates (5, 10, 20, 30, 50, and 100 mV s^{-1}) *vs.* Ag/AgCl over the potential window from 0 to 0.6 V at room temperature. Each film yields a pair of oxidation and reduction peaks in the anodic and cathodic sweeps related to Ni^{2+}/Ni^{3+} activation also Cu^{1+}/Cu^{2+}.[39] Ni and Cu species can simultaneously contribute to oxidation by offering two electroactive centers to enrich the redox reactions. This supports the electrochemical activity of thin film materials for energy conversion applications. Compared to the other thin films, NiO–Cu 1200 sample showed a superior current density, which is discernible from the results in (Table 4). From Fig. 7, it is seen that with increasing the deposition time (film thickness), the anodic and cathodic current densities have been increased.

The observed electrocatalytic activity enhancement may be due to increased active sites and deposited materials.

Fig. 8 shows the linear dependency of the redox peaks (anodic and cathodic) current densities of each film with the square root of the scan rate (5–100 mV s^{-1}). The results show that increasing the scan rate increases the oxidation–reduction reaction, and the electrochemical process is regulated by OH^-

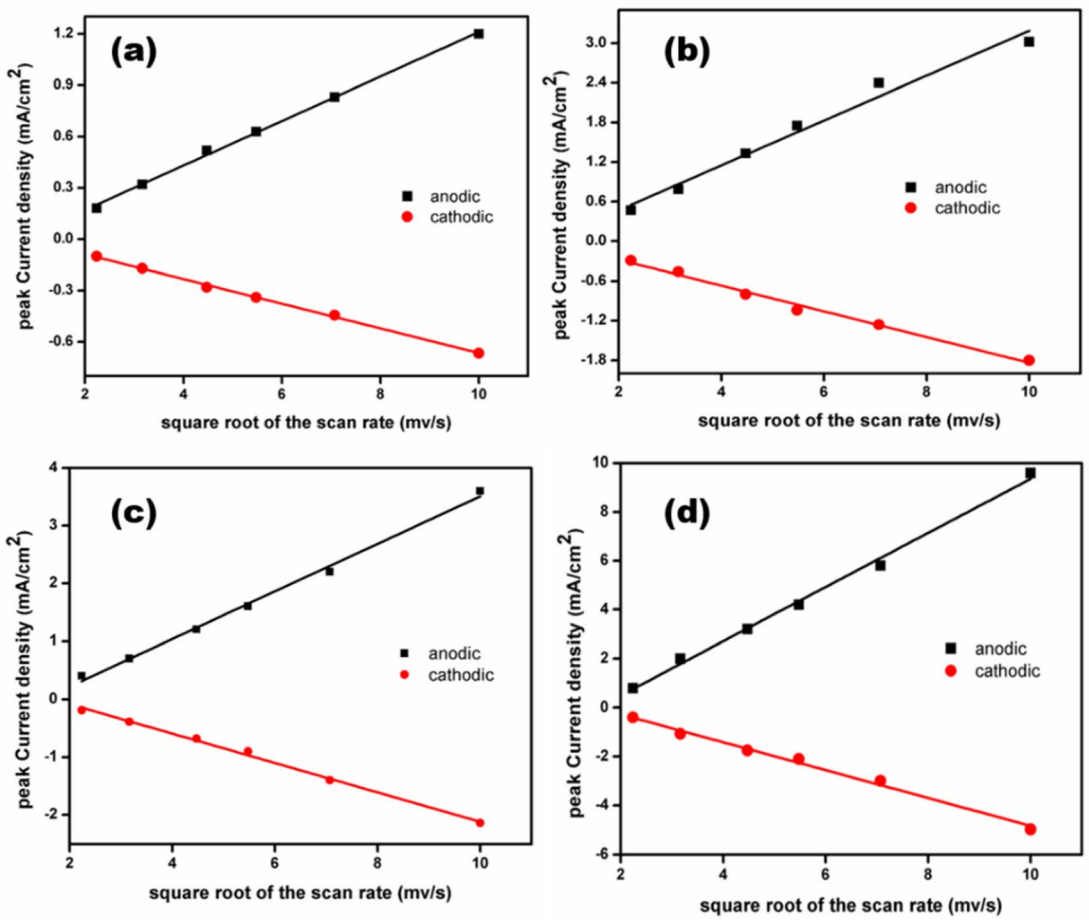

Fig. 8 The relationship between current density with the square root of the scan rate for anode and cathode (a) NiO–Cu 300, (b) NiO–Cu 600, (c) NiO–Cu 900, and (d) NiO–Cu 1200.

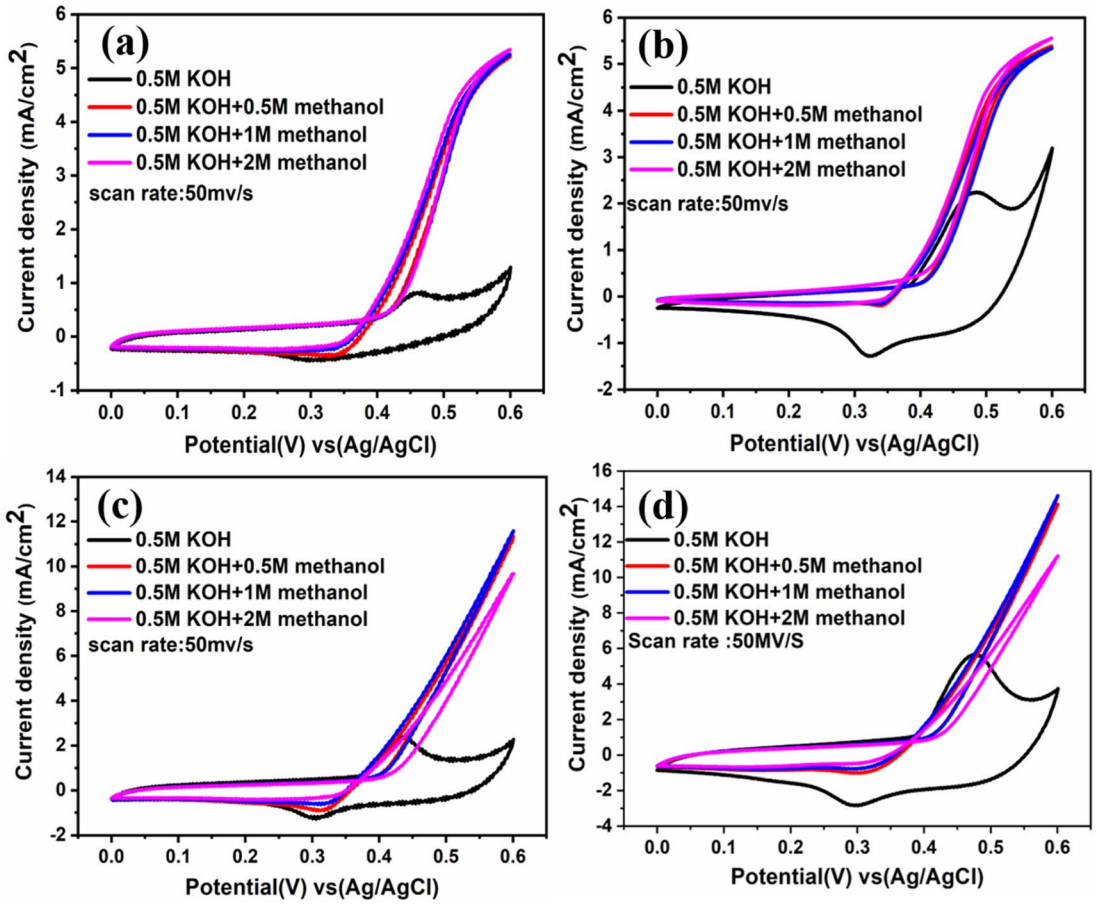

Fig. 9 CVs at different concentrations of CH_3OH at scan rate 50 mV s^{-1} (a) NiO–Cu 300, (b) NiO–Cu 600, (c) NiO–Cu 900, (d) NiO–Cu 1200.

migration into the pores cavities.[11] Based on Fig. 7 and 8, it is clear that NiO–Cu 1200 is superior in the redox reactions at different scan rates due to a large amount of NiO doped by copper spread on the FTO surface, improving catalytic activity due to increasing the diffusion rate of OH^- ions on the surface.

3.5. Electrocatalytic of methanol oxidation

The electrochemical performances of the synthesized films toward methanol oxidation in a basic medium of different methanol concentrations (0.5, 1, 2 M) are presented in Fig. 9. The cyclic voltammetry measurements over the potential window from 0 to 0.6 V *vs.* Ag/AgCl at a scan rate of 50 mV s^{-1} are displayed. All films exhibit electrochemical activity when methanol is added, even with a lower concentration of methanol (0.5 M). This is due to the presence of $Ni(OH)_2$ (ref. 26) species which help the movement of OH^- from $Ni(OH)_2$ to the nearby nanocrystals and create new active sites for adsorption, furthermore removing carbonaceous poisons CO from the surface of the Catalyst, both of which raise electrocatalytic activity,[6] in addition to transformation Cu to Cu^{2+}.[39]

Additionally, each film was studied at different scan rates in different concentrations of methanol (0.5, 1, and 2 M) as indicated in Fig. S4(a–c), S5(a–c), S6(a–c), and S7(a–c),† which appear a direct relationship between the current density and the scan rate. From Fig. S7,† it was observed that NiO–Cu 1200 has the lowest onset potential and the highest activity (current density), which means that increasing the thickness intensity of the deposited Cu-doped NiO film, increases the diffusion rate of methanol in addition to increasing the active sites. The rising

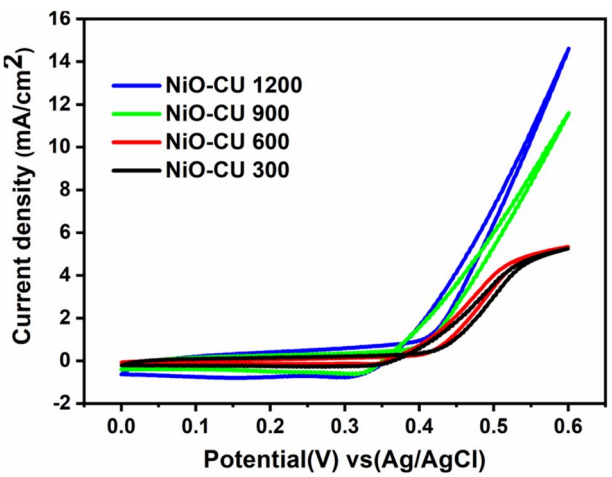

Fig. 10 Cyclic voltammograms of thin films in 0.5 M KOH + 1 M methanol solution with a scan rate of 50 mV s^{-1} at room temperature.

thickness of films forming many layers resulted in the high ratio of Ni^{2+}/Ni^{3+} and Cu^{2+} ions, which enhanced mass transport and electron transfer. As demonstrated in Fig. 9(a and b), the onset potential values for synthesized films before and after methanol addition relocated to more negative values when increasing methanol concentrations. When the onset potential is more negative for reactions at the anode, this refers to low over-potential and high electrochemical activity.[40] The current density recorded the highest intensity during the measurements in 1 M methanol, so the results were compared in Fig. 10 at a scan rate of 50 mV s^{-1}, which shows that the NiO–Cu 1200 is three times higher than the NiO–Cu 300.

As a comparision with the previously reported catalysts, Table 5 reported the performance comparison between the prepared Cu-doped NiO films and the similar transition metal catalysts reported in the literature.

Fig. 11(a) displays the electrochemical impedance spectroscopy (EIS) recorded in 1 M KOH containing 1 M methanol at 0.6 V *vs.* Ag/Ag Cl. According to the mechanism of methanol oxidation in alkaline media, as mentioned in (ref. 45 and 46), the following general equations: suggest that numerous processes are involved in MOR. As a result, the EIS spectra may have different properties.

$$M + OH^- \rightarrow M - (OH)_{ads} + e^- \quad (9)$$

$$M - (CH_3OH)_{ads} + 4OH^- \rightarrow M - (CO)_{ads} + 4H_2O + 4e^- \quad (10)$$

$$M - (CO)_{ads} + M - (OH)_{ads} + OH^- \rightarrow 2M + CO_2 + H_2O + e^- \quad (11)$$

where M represents an active site at the surface of the electrode.

In eqn (9), the oxidative hydroxyl ion is adsorbed. The process of dehydrogenating produces adsorbed carbon monoxide by the adsorbed methanol, as shown in eqn (10) lastly, eqn (11) shows how to produce carbon dioxide and regenerate active catalytic sites. It's clear that NiO–Cu 1200 exhibits the smallest semicircle diameter, about 16 ohms, because it has small interfacial charge transfer resistance compared to the other films, demonstrating improved charge transfer kinetics throughout the MOR process. This result agrees with cyclic voltammograms in Fig. 10. The used equivalent circuits are exhibited inside Fig. 11(a). The circuit consists of two parts: the first part is the R_s is the electrolyte's resistance, CPE is the constant phase element, and R_{ct} is the charge transfer resistance. The second part is associated with the intermediate adsorption rate (R_{ads}) and adsorption constant phase element (CPE_{ads}). The fitting results are depicted in Table 6. The charge transfer resistance of the films decreased by increasing the film thickness, where charges can move easily and quickly during the reaction because of increasing the amount of (Ni^{2+}/Ni^{3+}) and (Cu^{2+}), which act as the active site for the reaction.[45]

To evaluate the long-term stabilities of the deposited films as electrocatalysts for the MOR, chronoamperometry testing was

Table 5 Comparison of previously reported catalysts for similar catalysts

Catalysts	Methods of preparation	Morphology	Current density (mA cm^{-2})	Onset potential	Ref.
NiO–Cu 1200	Co-sputtering deposition	Thin film	15.3	0.37	This work
Cu-doped NiO	Sol–gel	Nano-flakes	0.4	0.41	41
NiO	Hydrothermal	Nanosheet	9.5	0.5	42
NiO	Hydrothermal	Nanoflake	1.9	0.87	43
GC/NiO_x	Potentiostatic deposition	Nanoparticles	0.5	0.44	22
$NiCu_2O_4$	Combustion route	Particles	8	0.8	44

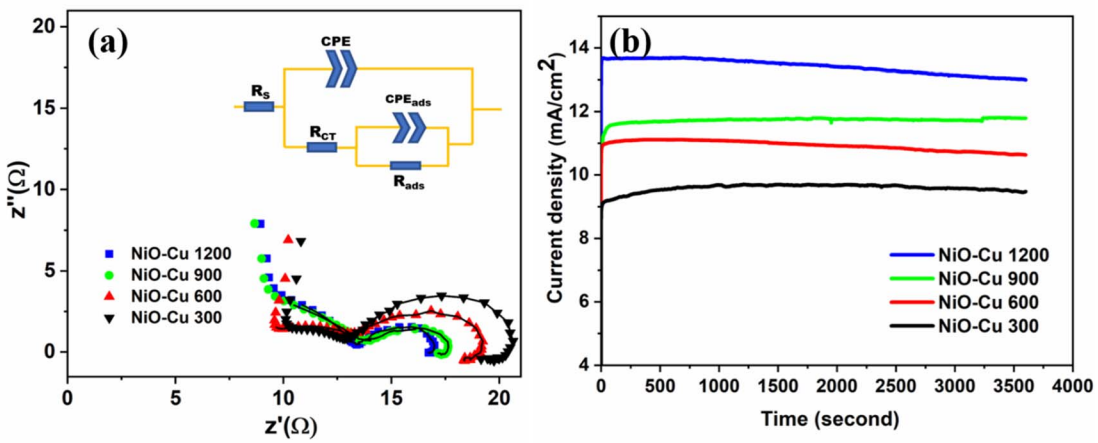

Fig. 11 (a) Nyquist plots for the oxidation reaction, (b) chronoamperometric response for the films, at 0.60 V using 1 M methanol.

Table 6 Values of EIS fitting

The prepared films	R_s	R_{CT}	R_{ads}	CPE		CPE_{ads}	
				CPE-T	CPE-P	CPE-T	CPE-P
NiO-Cu 300	9.6	16.61	4.63	1.80×10^{-4}	0.85	1.51×10^{-3}	0.85
NiO-Cu 600	9.1	15.12	4.02	9.91×10^{-4}	0.80	2.1×10^{-3}	0.86
NiO-Cu 900	8.71	14.34	3.32	1.05×10^{-5}	0.85	4.61×10^{-3}	0.80
NiO-Cu 1200	8.00	13.22	3.23	5.36×10^{-5}	0.90	4.8×10^{-3}	0.92

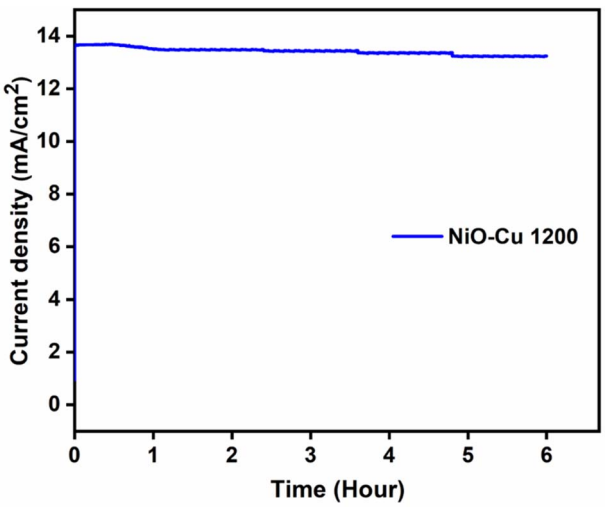

Fig. 12 Chronoamperometric measurement for NiO–Cu-1200, at 0.6 V using 1 M methanol for 6 h.

performed at a constant voltage of 0.6 V on all catalysts for 3600 s, as shown in Fig. 11b. It is revealed that NiO–Cu 1200 still shows the highest activity over the test period in agreement with the previous measurements, may be related to its higher thickness, increasing the active sides also the nature of the surface which appears more roughness as obvious in FESEM images, enhancing the catalytic efficiency by Stimulating the rapid conversion of adsorbed intermediates into materials.

The long term stability test was conducted for NiO–Cu 1200 film through recoding the chronoamperometry at 0.6 V for 6 hours as displayed in Fig. 12. 5% current density loss from the initial current density values after 6 h as an electrocatalyst for MOR in 1 M methanol solution. This is a promising stability result as the electrocatalyst can retain more than 95% of its efficiency.

4. Conclusion

The co-sputtering deposition method has been utilized successfully to prepare Cu-doped NiO thin films at various deposition times (300, 600, 900, and 1200 seconds) on FTO as a conductive substrate. Then, the prepared films were used as electrocatalysts for methanol oxidation in a basic medium. The characterization analysis showed that the thickness increase with increasing the deposition time, as confirmed by FESEM images. The prepared films experienced high purity with good crystallinity, as detected by XRD and EDX. The crystal size increased from 52, 57, and 69 to 75 nm, with increasing the deposition time from 300, 600, and 900 to 1200 seconds, respectively. The electrochemical activity for MOR demonstrated that the prepared films are promising for using as electrocatalysts because they have high stability and good performance for charge transfer during the oxidation process. Otherwise, the thickness of films affects the current density values, which increase with the thin film's thickness. From the CV conducted scan rate 50 mV s^{-1} in 1 M methanol, the current density values were 5.9, 6, 12, and 15 mA cm^{-2} for the deposited samples at 300, 600, 900, and 1200 seconds respectively. Moreover, the onset potential decreased with increasing the film thickness. These findings may open a new thin film deposition technology era to adapt the performance of different electrocatalysts for different electrocatalytic applications.

Conflicts of interest

We declare that we have no known competing financial interests or personal relationships that could have appeared to influence the work reported in this paper.

References

1 R. Artal, A. Serrà, J. Michler, L. Philippe and E. Gómez, Electrodeposition of mesoporous ni-rich ni-pt films for highly efficient methanol oxidation, *Nanomaterials*, 2020, **10**, 1–17, DOI: 10.3390/nano10081435.

2 W. Yang, X. Yang, J. Jia, C. Hou, H. Gao, Y. Mao, C. Wang, J. Lin and X. Luo, Oxygen vacancies confined in ultrathin nickel oxide nanosheets for enhanced electrocatalytic methanol oxidation, *Appl. Catal., B*, 2019, **244**, 1096–1102, DOI: 10.1016/j.apcatb.2018.12.038.

3 R. M. A. Tehrani and S. AbGhani, The nanocrystalline nickel with catalytic properties on methanol oxidation in alkaline medium, *Fuel Cells*, 2009, **9**, 579–587, DOI: 10.1002/fuce.200800122.

4 V. Latyshev, H. You, A. Kovalcikova and V. Komanicky, Enhancing catalytic activity of rhodium towards methanol electro-oxidation in both acidic and alkaline media by alloying with iron, *Electrochim. Acta*, 2020, **330**(10), 1351178, DOI: 10.1016/j.electacta.2019.135178.

5 E. H. Yu, K. Scott and R. W. Reeve, A study of the anodic oxidation of methanol on Pt in alkaline solutions, *J.*

Electroanal. Chem., 2003, **547**, 17–24, DOI: 10.1016/S0022-0728(03)00172-4.

6 W. Huang, H. Wang, J. Zhou, J. Wang, P. N. Duchesne, D. Muir, P. Zhang, N. Han, F. Zhao, M. Zeng, J. Zhong, C. Jin, Y. Li, S. T. Lee and H. Dai, Highly active and durable methanol oxidation electrocatalyst based on the synergy of platinum-nickel hydroxide-graphene, *Nat. Commun.*, 2015, **6**, 1–8, DOI: 10.1038/ncomms10035.

7 H. M. Villullas, F. I. Mattos-Costa and L. O. S. Bulhões, Electrochemical oxidation of methanol on Pt nanoparticles dispersed on RuO_2, *J. Phys. Chem. B*, 2004, **108**, 12898–12903, DOI: 10.1021/jp049662r.

8 T. Maiyalagan and F. N. Khan, Electrochemical oxidation of methanol on Pt/V_2O_5-C composite catalysts, *Catal. Commun.*, 2009, **10**, 433–436, DOI: 10.1016/j.catcom.2008.10.011.

9 S. Sakong and A. Groß, The Importance of the Electrochemical Environment in the Electro-Oxidation of Methanol on Pt(111), *ACS Catal.*, 2016, **6**, 5575–5586, DOI: 10.1021/acscatal.6b00931.

10 S. Gamil, M. Antuch, I. T. Zedan and W. M. A. El Rouby, 3D NiCr-layered double hydroxide/reduced graphene oxide sand rose-like structure as bifunctional electrocatalyst for methanol oxidation, *Colloids Surf., A*, 2020, **602**, 125067, DOI: 10.1016/j.colsurfa.2020.125067.

11 A. Zaher, W. M. A. El Rouby and N. A. M. Barakat, Tungsten incorporation in nickel doped carbon nanofibers as efficient electrocatalyst for ethanol oxidation, *Fuel*, 2020, 280, DOI: 10.1016/j.fuel.2020.118654.

12 A. Hamdedein, W. M. A. El Rouby, M. D. Khan, M. M. EL-Deeb, A. A. Farghali, M. H. Khedr and N. Revaprasadu, Synthesis and characterization of Ni/NiCo2O4 modified electrode for methanol electro-catalytic oxidation, *IOP Conf. Ser.: Mater. Sci. Eng.*, 2021, **1046**, 012027, DOI: 10.1088/1757-899X/1046/1/012027.

13 S. G. Peera, T. G. Lee and A. K. Sahu, Pt-rare earth metal alloy/metal oxide catalysts for oxygen reduction and alcohol oxidation reactions: an overview, *Sustainable Energy Fuels*, 2019, **3**, 1866–1891, DOI: 10.1039/c9se00082h.

14 J. Xu, X. Liu, Y. Chen, Y. Zhou, T. Lu and Y. Tang, Platinum-Cobalt alloy networks for methanol oxidation electrocatalysis, *J. Mater. Chem.*, 2012, **22**, 23659–23667, DOI: 10.1039/c2jm35649j.

15 X. Q. Wu, J. Zhao, Y. P. Wu, W. W. Dong, D. S. Li, J. R. Li and Q. Zhang, Ultrafine Pt Nanoparticles and Amorphous Nickel Supported on 3D Mesoporous Carbon Derived from Cu-Metal-Organic Framework for Efficient Methanol Oxidation and Nitrophenol Reduction, *ACS Appl. Mater. Interfaces*, 2018, **10**, 12740–12749, DOI: 10.1021/acsami.8b01970.

16 R. M. A. Hameed, A. E. Fetohi, R. S. Amin and K. M. El-khatib, Promotion effect of manganese oxide on the electrocatalytic activity of Pt/C for methanol oxidation in acid medium, *Appl. Surf. Sci.*, 2015, **359**, 651–663.

17 L. Chen, X. Liang, X. Li, J. Pei, H. Lin, D. Jia, W. Chen, D. Wang and Y. Li, Promoting electrocatalytic methanol oxidation of platinum nanoparticles by cerium modification, *Nano Energy*, 2020, **73**, 104784, DOI: 10.1016/j.nanoen.2020.104784.

18 Z. Ji, G. Zhu, X. Shen, H. Zhou, C. Wu and M. Wang, Reduced graphene oxide supported FePt alloy nanoparticles with high electrocatalytic performance for methanol oxidation, *New J. Chem.*, 2012, **36**, 1774–1780, DOI: 10.1039/c2nj40133a.

19 Q. Wang, Z. Zhao, Y. Jia, M. Wang, W. Qi, Y. Pang, J. Yi, Y. Zhang, Z. Li and Z. Zhang, Unique Cu@CuPt Core-Shell Concave Octahedron with Enhanced Methanol Oxidation Activity, *ACS Appl. Mater. Interfaces*, 2017, **9**, 36817–36827, DOI: 10.1021/acsami.7b11268.

20 H. k. El Emam, A. Abdelwahab, S. I. El-Dek and W. M. A. El Rouby, Performance of Ni-doped $BaTiO_3$ Hollow Porous Spheres Supported Reduced Graphene Oxide as an Efficient Bifunctional Electrocatalyst for Oxygen Evolution Reaction and Oxygen Reduction Reaction, *Appl. Surf. Sci.*, 2023, **618**, 156599, DOI: 10.1016/j.apsusc.2023.156599.

21 M. Roca-Ayats, G. García, J. L. Galante, M. A. Peña and M. V. Martínez-Huerta, TiC, TiCN, and TiN supported Pt electrocatalysts for CO and methanol oxidation in acidic and alkaline media, *J. Phys. Chem. C*, 2013, **117**, 20769–20777, DOI: 10.1021/jp407260v.

22 R. H. Tammam, A. M. Fekry and M. M. Saleh, Electrocatalytic oxidation of methanol on ordered binary catalyst of manganese and nickel oxide nanoparticles, *Int. J. Hydrogen Energy*, 2015, **40**, 275–283, DOI: 10.1016/j.ijhydene.2014.03.109.

23 T. Frelink, W. Visscher and J. A. R. van Veen, On the role of Ru and Sn as promotors of methanol electro-oxidation over Pt, *Surf. Sci.*, 1995, **335**, 353–360, DOI: 10.1016/0039-6028(95)00412-2.

24 J. H. Yang, X. Song, X. Zhao, Y. Wang, Y. Yang and L. Gao, Nickel phosphate materials regulated by doping cobalt for urea and methanol electro-oxidation, *Int. J. Hydrogen Energy*, 2019, **44**, 16305–16314, DOI: 10.1016/j.ijhydene.2019.05.016.

25 E. Antolini, J. R. C. Salgado and E. R. Gonzalez, The methanol oxidation reaction on platinum alloys with the first row transition metals: the case of Pt-Co and -Ni alloy electrocatalysts for DMFCs: a short review, *Appl. Catal., B*, 2006, **63**, 137–149, DOI: 10.1016/j.apcatb.2005.09.014.

26 M. A. A. Rahim, R. M. A. Hameed and M. W. Khalil, Nickel as a catalyst for the electro-oxidation of methanol in alkaline medium, *J. Power Sources*, 2004, **134**, 160–169, DOI: 10.1016/j.jpowsour.2004.02.034.

27 K. H. Luo, C. K. Cheng, J. Y. Lin, C. H. Huang, T. K. Yeh and C. K. Hsieh, Highly-porous hierarchically microstructure of graphene-decorated nickel foam supported two-dimensional quadrilateral shapes of cobalt sulfide nanosheets as efficient electrode for methanol oxidation, *Surf. Coat. Technol.*, 2020, **393**, 125850, DOI: 10.1016/j.surfcoat.2020.125850.

28 I. S. Pieta, A. Rathi, P. Pieta, R. Nowakowski, M. Hołdynski, M. Pisarek, A. Kaminska, M. B. Gawande and R. Zboril, Electrocatalytic methanol oxidation over Cu, Ni and bimetallic Cu-Ni nanoparticles supported on graphitic carbon nitride, *Appl. Catal., B*, 2019, **244**, 272–283, DOI: 10.1016/j.apcatb.2018.10.072.

29 A. Zhang, Y. Liang, H. Zhang, Z. Geng and J. Zeng, Doping regulation in transition metal compounds for electrocatalysis, *Chem. Soc. Rev.*, 2021, **50**, 9817–9844, DOI: **10.1039/d1cs00330e**.

30 I. Soni, P. Kumar and G. Kudur Jayaprakash, Recent advancements in the synthesis and electrocatalytic activity of two-dimensional metal–organic framework with bimetallic nodes for energy-related applications, *Coord. Chem. Rev.*, 2022, **472**, 214782, DOI: **10.1016/j.ccr.2022.214782**.

31 A. Chalgin, C. Song, P. Tao, W. Shang, T. Deng and J. Wu, Effect of supporting materials on the electrocatalytic activity, stability and selectivity of noble metal-based catalysts for oxygen reduction and hydrogen evolution reactions, *Prog. Nat. Sci.: Mater. Int.*, 2020, **30**, 289–297, DOI: **10.1016/j.pnsc.2020.01.003**.

32 F. M. Doyle and Z. Liu, The effect of triethylenetetraamine (Trien) on the ion flotation of Cu^{2+} and Ni^{2+}, *J. Colloid Interface Sci.*, 2003, **258**, 396–403, DOI: **10.1016/S0021-9797(02)00092-9**.

33 J. S. J. Hargreaves, Some considerations related to the use of the Scherrer equation in powder X-ray diffraction as applied to heterogeneous catalysts, *Catal., Struct. React.*, 2016, **2**, 33–37, DOI: **10.1080/2055074X.2016.1252548**.

34 K. Venkateswarlu, M. Sandhyarani, T. A. Nellaippan and N. Rameshbabu, Estimation of Crystallite Size, Lattice Strain and Dislocation Density of Nanocrystalline Carbonate Substituted Hydroxyapatite by X-ray Peak Variance Analysis, *Procedia Mater. Sci.*, 2014, **5**, 212–221, DOI: **10.1016/j.mspro.2014.07.260**.

35 K. S. Babu, T. R. Kumar, P. Haridoss and C. Vijayan, Effect of the organic solvent on the formation and stabilization of CdS and PbS nanoclusters, *Talanta*, 2005, **66**, 160–165, DOI: **10.1016/j.talanta.2004.11.002**.

36 M. M. Abbas, A. Ab-M. Shehab, A. K. Al-Samuraee and N. A. Hassan, Effect of deposition time on the optical characteristics of chemically deposited nanostructure PBS thin films, *Energy Procedia*, 2011, **6**, 241–250, DOI: **10.1016/j.egypro.2011.05.028**.

37 M. Ali Yildirim and A. Ateş, Influence of films thickness and structure on the photo-response of ZnO films, *Opt. Commun.*, 2010, **283**, 1370–1377, DOI: **10.1016/j.optcom.2009.12.009**.

38 K. Mageshwari and R. Sathyamoorthy, Physical properties of nanocrystalline CuO thin films prepared by the SILAR method, *Mater. Sci. Semicond. Process.*, 2013, **16**, 337–343, DOI: **10.1016/j.mssp.2012.09.016**.

39 I. Valov and W. D. Lu, Nanoscale electrochemistry using dielectric thin films as solid electrolytes, *Nanoscale*, 2016, **8**, 13828–13837, DOI: **10.1039/c6nr01383j**.

40 G. Zhang, Y. Li, Y. Zhou and F. Yang, NiFe Layered-Double-Hydroxide-Derived NiO-$NiFe_2O_4$/Reduced Graphene Oxide Architectures for Enhanced Electrocatalysis of Alkaline Water Splitting, *ChemElectroChem*, 2016, **3**, 1927–1936, DOI: **10.1002/celc.201600301**.

41 M. A. Hefnawy, S. A. Fadlallah, R. M. El-Sherif and S. S. Medany, Synergistic effect of Cu-doped NiO for enhancing urea electrooxidation: comparative electrochemical and DFT studies, *J. Alloys Compd.*, 2022, **896**, 162857, DOI: **10.1016/j.jallcom.2021.162857**.

42 Z. Jia, S. R. Rondiya, R. W. Cross, C. Wang, N. Y. Dzade and C. Zhang, Highly active methanol oxidation electrocatalyst based on 2D NiO porous nanosheets:a combined computational and experimental study, *Electrochim. Acta*, 2021, **394**, 139143, DOI: **10.1016/j.electacta.2021.139143**.

43 M. U. Anu Prathap and R. Srivastava, Synthesis of $NiCo_2O_4$ and its application in the electrocatalytic oxidation of methanol, *Nano Energy*, 2013, **2**, 1046–1053, DOI: **10.1016/j.nanoen.2013.04.003**.

44 N. K. Naveen, L. R. Harishitha and B. Neppolian, Facile synthesis of boron doped $NiCu_2O_4$ for efficient methanol oxidation: selective towards value-added formate formation, *Ceram. Int.*, 2022, **48**, 29025–29030, DOI: **10.1016/j.ceramint.2022.04.248**.

45 T. Iwasita, Electrocatalysis of methanol oxidation, *Electrochim. Acta*, 2002, **47**, 3663–3674, DOI: **10.1016/S0013-4686(02)00336-5**.

46 I.-M. Hsing, X. Wang and Y.-J. Leng, Electrochemical Impedance Studies of Methanol Electro-oxidation on Pt/C Thin Film Electrode, *J. Electrochem. Soc.*, 2002, **149**, A615, DOI: **10.1149/1.1467940**.